Electronic Supplementary Information for

Two C_{2v} Symmetry Dysprosium(III) Single-Molecule Magnets with Effective Energy Barriers over 600 K

Xixi Meng,[a] Mengmeng Wang,[a] Xiaoshuang Gou,[a] Wenlong Lan,[a] Kexin Jia,[a] Yu-Xia Wang,[a] Yi-Quan Zhang,[b] Wei Shi*[a] and Peng Cheng[a]*

[a]Department of Chemistry and Key Laboratory of Advanced Energy Materials Chemistry (MOE), College of Chemistry, Nankai University, Tianjin 300071, China.

[b]Jiangsu Key Lab for NSLSCS, School of Physical Science and Technology, Nanjing Normal University, Nanjing 210023, P. R. China

E-mail: shiwei@nankai.edu.cn; zhangyiquan@njnu.edu.cn

Table of Contents

S1. Experimental Section

X-ray Crystallography. The single crystal of **1** or **2** covered with grease was mounted on a Rigaku XtaLAB Mini II single-crystal diffractometer with graphite-monocromatic Mo-Kα radiation (λ = 0.71073 Å). The data were measured by ω-scan mode. The structures were solved by the direct methods with SHELXS and refined by full-matrix least-squares techniques against F^2 (SHELXL-2014) using the program package Olex-2 software.[1] All the non-hydrogen atoms were refined with anisotropic thermal parameters. All hydrogen atoms were placed in calculated positions and a riding model was used. Crystallographic data and refinement for **1** and **2** are listed in Table S1†. CCDC 2055350 and 2055351 for **1** and **2**, respectively, are offered in the Cambridge Crystallographic Data Centre.

Computational Details. Complete-active-space self-consistent field (CASSCF) calculations on mononuclear **1** and **2** on the basis of single-crystal X-ray determined geometry have been carried out with MOLCAS 8.4[2] program package (see Fig. S25† for the calculated complete structures of **1** and **2**). The basis sets for all atoms are atomic natural orbitals from the MOLCAS ANO-RCC library: ANO-RCC-VTZP for Dy^{III}; VTZ for close N, O, Cl and Br; VDZ for distant atoms. The calculations employed the second order Douglas-Kroll-Hess Hamiltonian, where scalar relativistic contractions were considered in the basis set and the spin-orbit couplings were handled separately in the restricted active space state interaction (RASSI-SO) procedure. Active electrons in 7 active orbitals include all *f* electrons (CAS(9 in 7) in the CASSCF calculation. To exclude all the doubts, we calculated all the roots in the active space. We have mixed the maximum number of spin-free state which was possible with our hardware (all from 21 sextets, 128 from 224 quadruplets, 130 from 490 doublets for Dy^{III}. SINGLE_ANISO[3] program was used to obtain the energy levels, ***g*** tensors, magnetic axes, et al., based on the above CASSCF/RASSI-SO calculations.

Material and methods. Anhydrous $DyCl_3$ and $DyBr_3$ were purchased from Alfa Aesar and used as received. Ethanol, acetonitrile and tetrahydrofuran were dried using a commercial solvent purification system designed by MIKROUNA Solvent Systems

and stored over 4 Å molecular sieves. All reactions were performed in an argon filled glovebox or under an argon atmosphere using Schlenk techniques, and all operations described below were performed under aerobic conditions. The ligand 2,2'-(((pyridine-2,6-diylbis(methylene))bis((pyridin-2-yl-methyl)azanediyl))-bis(methylene))diphenol (H_2L) was prepared according to the reported methods.[4] Elemental analyses (C, H, N) were measured on a Perkin-Elmer elemental analyzer. The Fourier transform infrared (FTIR) spectra were measured in the range of 400-4000 cm^{-1} on a Bruker ALPHA FTIR spectrophotometer equipped with an attenuated total reflectance accessory. Powder X-ray diffraction (PXRD) measurements were carried out on a Rigaku Smartlab SE X-ray diffractometer using Cu-Kα radiation to verify the phase purity of the polycrystalline samples. Thermogravimetric analysis (TGA) was performed in a Mettler Toledo TGA 2 apparatus with a heating rate of 10 °C / min in nitrogen atmosphere. Magnetic measurements for all the samples were performed on a Quantum Design SQUID MPMS VSM magnetometer in the temperature range of 2-300 K. The measurements were performed on polycrystalline samples. The temperature dependences of the magnetization were conducted from 300 to 2 K in an applied 1000 Oe dc field, and the measured susceptibilities were corrected for the diamagnetic contribution of the sample holder and sample by using Pascal's tables. The field dependences of the magnetization were collected at several temperatures between 2 and 7 K with dc magnetic field up to 7 T. Alternating-current (ac) measurements were performed on at various frequencies ranging from 1 to 1000 Hz with a 3 Oe oscillating ac field.

Synthesis of [DyLCl]·CH_3CH_2OH (1). To a solution of $DyCl_3$ (27 mg, 0.1 mmol) and H_2L (53 mg, 0.1 mmol) in ethanol (3 mL), triethylamine (28 μL, 0.2 mmol) was dropwise added. After stirring for 30 min, the resulting mixture was filtrated, and the filtrate was left at room temperature for slow evaporation. Colorless block crystals available for single crystal X-ray diffraction formed after one days. The crystals were obtained by filtration in 56 % yield (based on Dy^{III} salts). Elemental analysis for **1**: Calcd (%): C 54.40, H 4.57, N 9.33; found: C 54.62, H 4.86, N 9.28. FTIR: 3435(w),

2968(w), 1593(m), 1476(s), 1439(s), 1291(s), 1156(w), 1051(m), 1005(s), 961(m), 879(m), 787(m), 771(s), 751(s), 582(s), 478(s) cm^{-1}.

Synthesis of [DyLBr]·2THF (**2**). To a solution of H_2L (53 mg, 0.1 mmol) in tetrahydrofuran (3 mL), triethylamine (28 μL, 0.2 mmol) was added. After stirring for 5 min, the anhydrous $DyBr_3$ (40 mg, 0.1 mmol) solid was added, which was sealed in a 10 mL vial at 65 °C for 12 h, and then slowly cooled to room temperature by 10 °C / h. Colorless block crystals were formed with a yield of 37% (based on Dy^{III} salts). Elemental analysis for **2**: Calcd (%): C 53.75, H 5.17, N 7.64; Found: C 53.96, H 5.63, N 7.57. FT-IR: 2933(w), 2675(w), 1595(m), 1476(s), 1442(s), 1295(s), 1159(w), 1067 (w), 1005(w), 960(w), 887(m), 842(w), 751(m), 582(w), 478(w) cm^{-1}.

S2. Structural figures

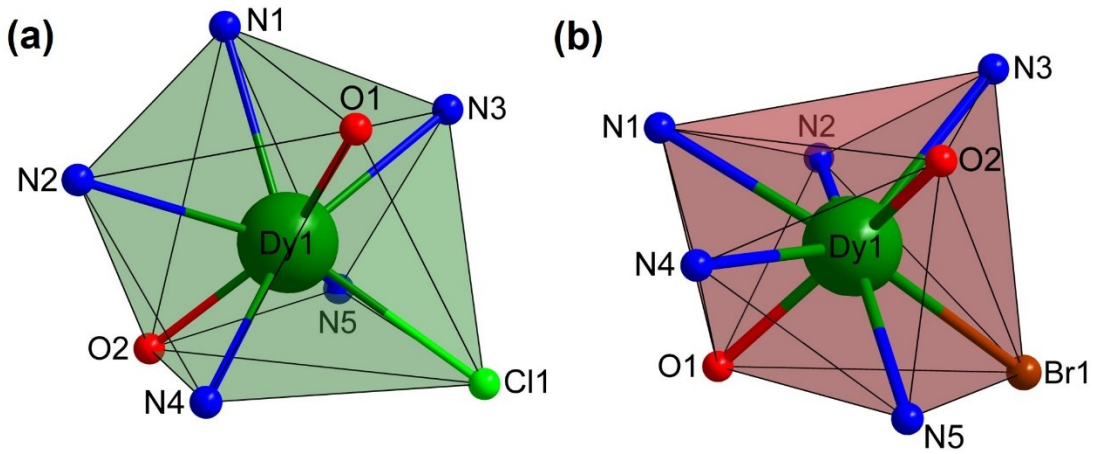

Fig. S1 The coordination environments of Dy^{III} ions in **1** (a) and **2** (b).

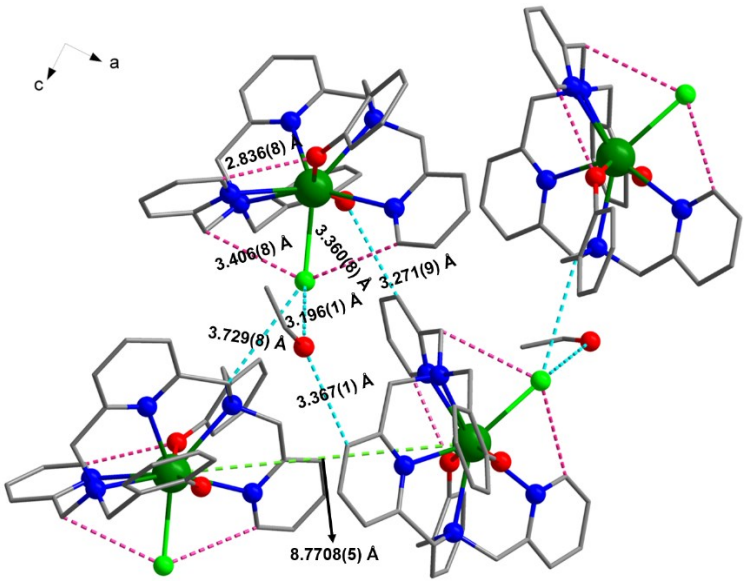

Fig. S2 Packing diagram of **1**. Hydrogen atoms and solvent molecules are omitted for clarity. Dy, green; N, blue; O, red; Cl, bright green; C, grey. The green, cyan and rosy dashed lines represent the distances between nearest neighboring Dy^{III} centers, intermolecular hydrogen bonds (O3···H3···Cl1 3.196(1) Å, C4···H4b···Cl1 3.729(8) Å, C18···H18···O3 3.367(1) Å, C30···H30···O1 3.271(9) Å) and intramolecular hydrogen bonds (C17···H17···Cl1 3.367(1) Å, C28···H28a···Cl1 3.406(8) Å, C33···H33···O2 2.836(8) Å), respectively.

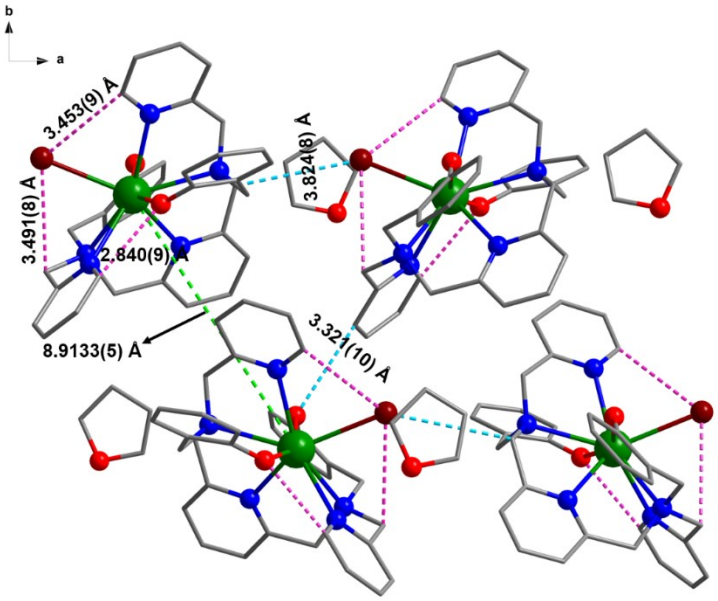

Fig. S3 Packing diagram of **2**. Hydrogen atoms are omitted for clarity. Dy, green; N, blue; O, red; Br, sorrel; C, grey. The green, cyan and violet dashed line represents the distances between nearest neighboring Dy^{III} centers, intermolecular hydrogen bonds (O10···H10···O1 3.321(10) Å, C20···H20a···Br1 3.824(8) Å, and intramolecular hydrogen bonds (C8···H8b···Br1 3.491(8) Å, C13···H13···O2 2.840(9) Å, C33···H33···Br1 3.453(9) Å), respectively.

S3. PXRD and TGA

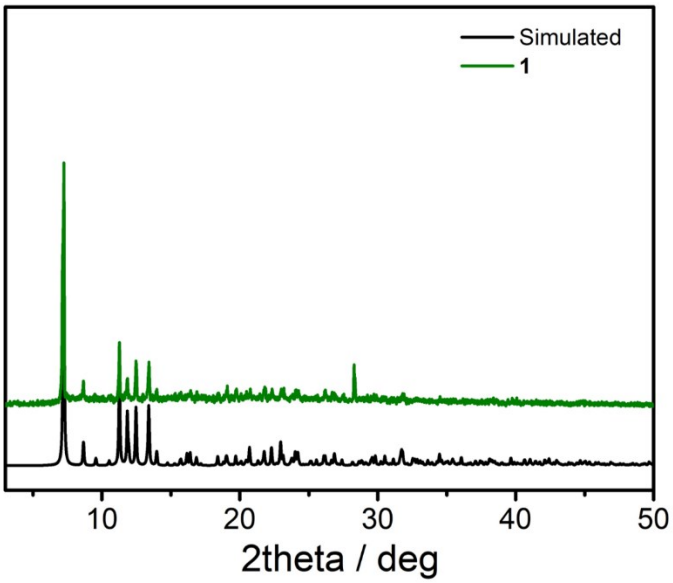

Fig. S4 PXRD pattern of **1**.

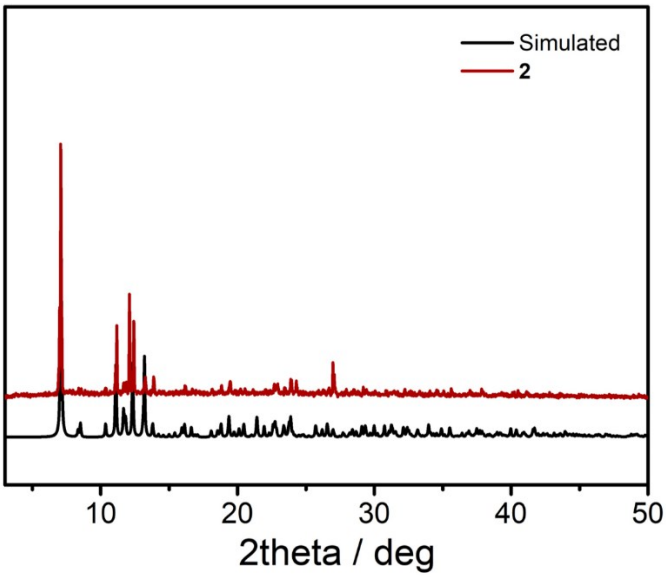

Fig. S5 PXRD pattern of **2**.

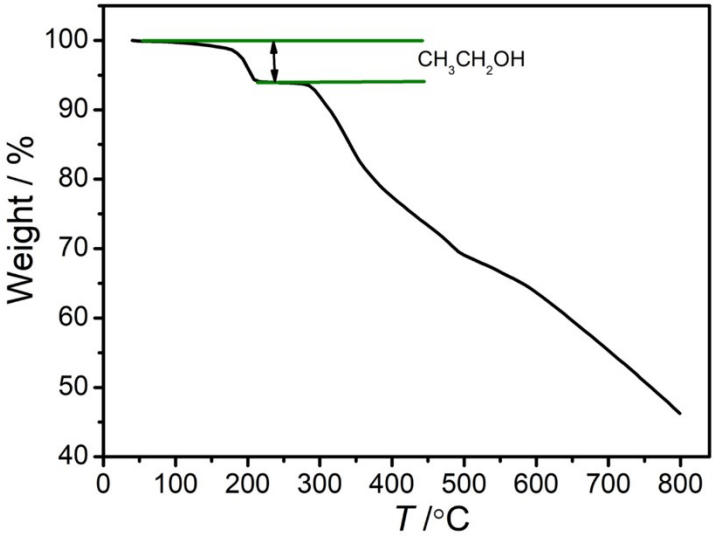

Fig. S6 TGA of **1**.

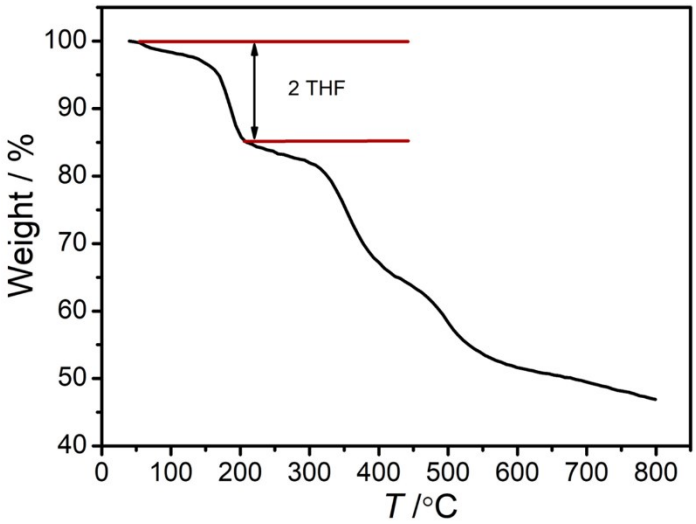

Fig. S7 TGA of **2**.

S4. Magnetic Characterizations

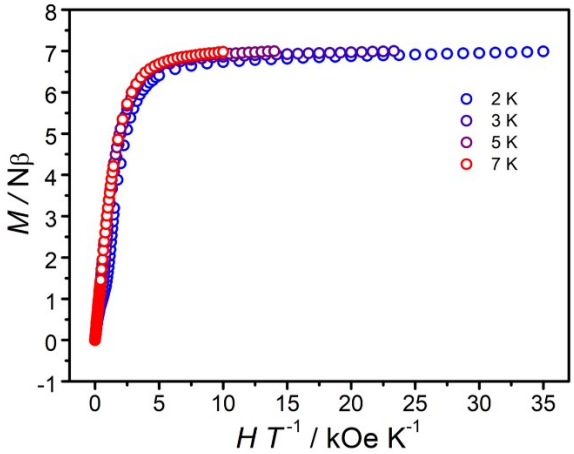

Fig. S8 Plots of the *M* vs. *H*/*T* of **1**.

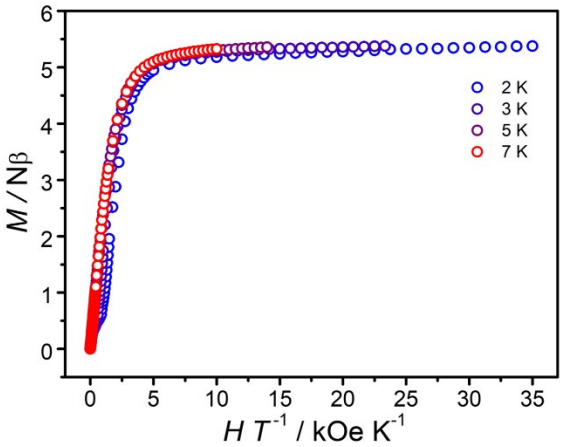

Fig. S9 Plots of the *M* vs. *H*/*T* of **2**.

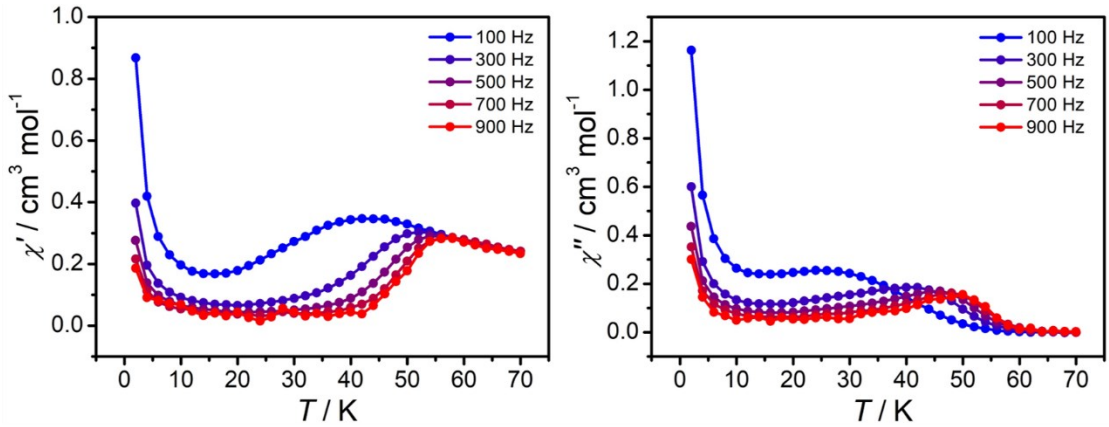

Fig. S10 Ac magnetic susceptibilities vs. temperature at given frequencies for **1** at H_{dc} = 0 Oe and H_{ac} = 3 Oe.

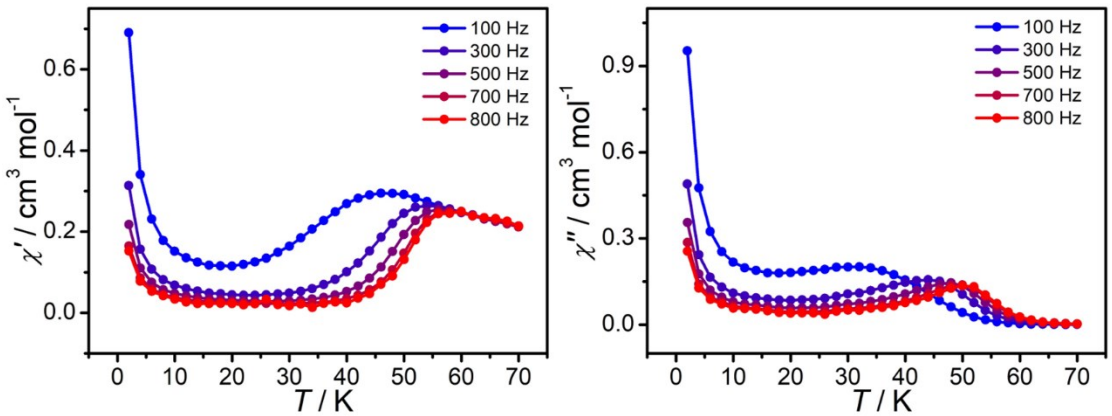

Fig. S11 Ac magnetic susceptibilities vs. temperature at given frequencies for **2** at H_{dc} = 0 Oe and H_{ac} = 3 Oe.

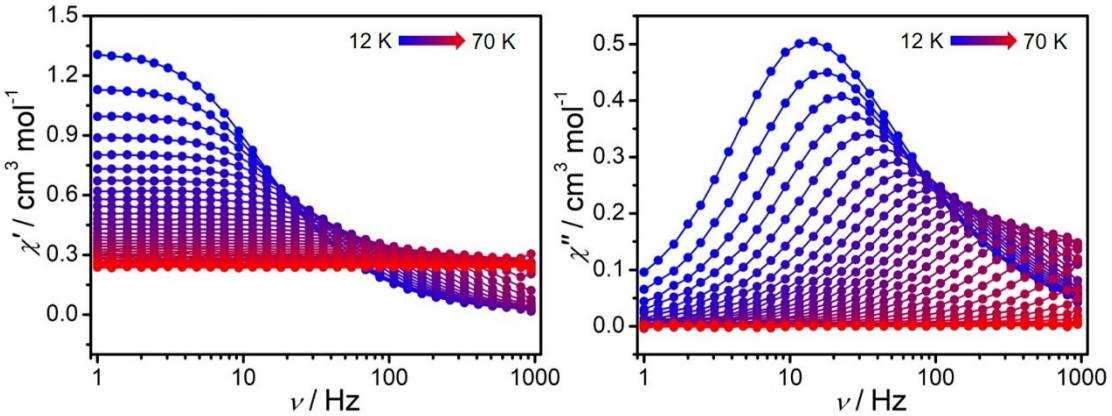

Fig. S12 Frequency dependence of ac susceptibilities of **1** at H_{dc} = 0 Oe and H_{ac} = 3 Oe.

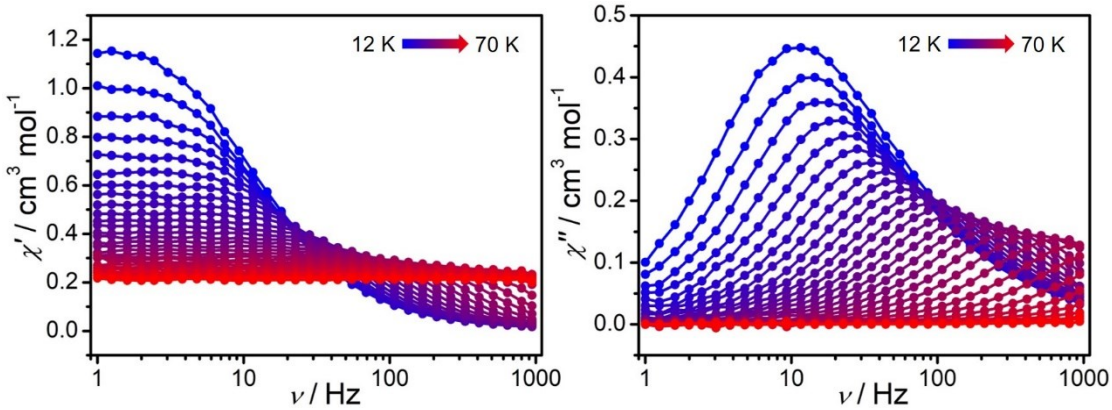

Fig. S13 Frequency dependence of ac susceptibilities of **2** at H_{dc} = 0 Oe and H_{ac} = 3 Oe.

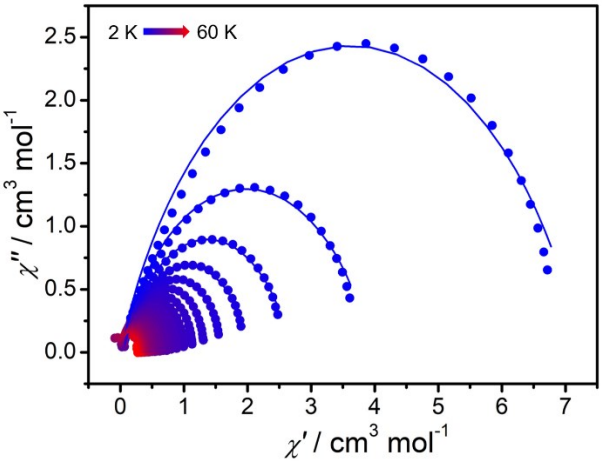

Fig. S14 Cole-Cole plots of **1**.

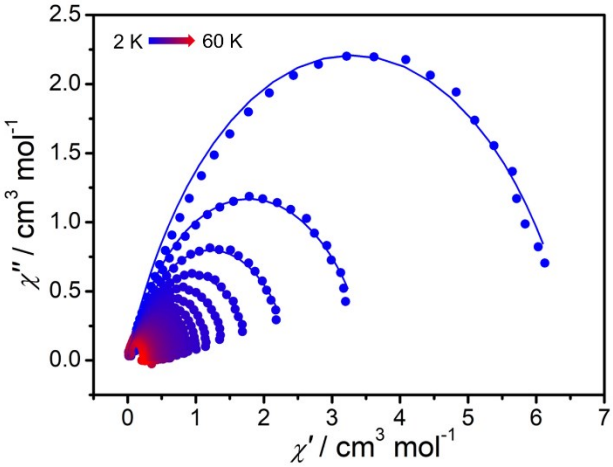

Fig. S15 Cole-Cole plots of **2**.

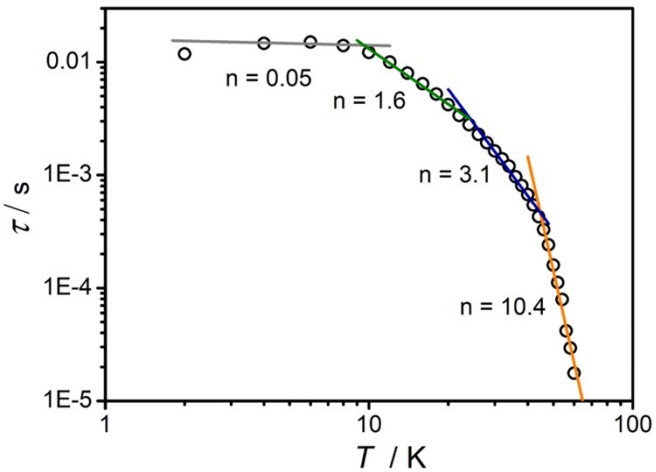

Fig. S16 The τ *versus* T^{-n} plot in a log-log scale for **1**.

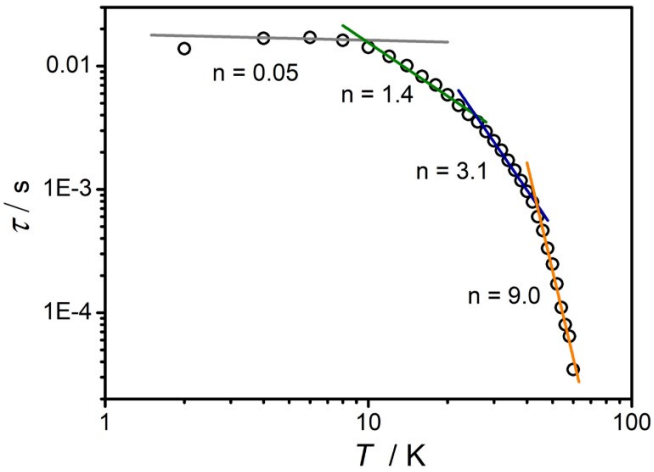

Fig. S17 The τ *versus* T^{-n} plot in a log-log scale for **2**.

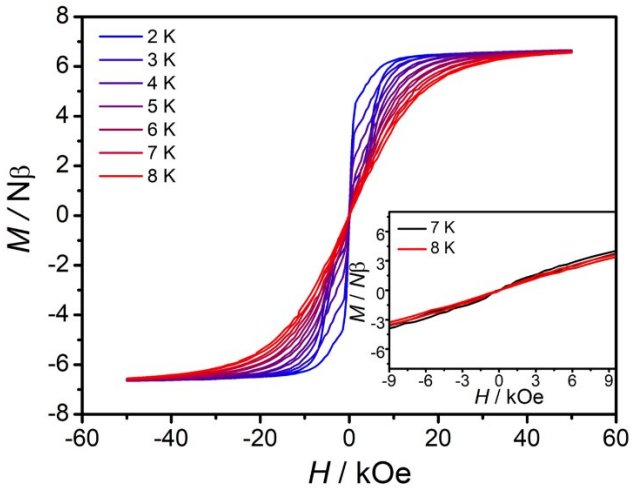

Fig. S18 Magnetic hysteresis loops of **1** at a field sweep rate of 0.02 T s^{-1}.

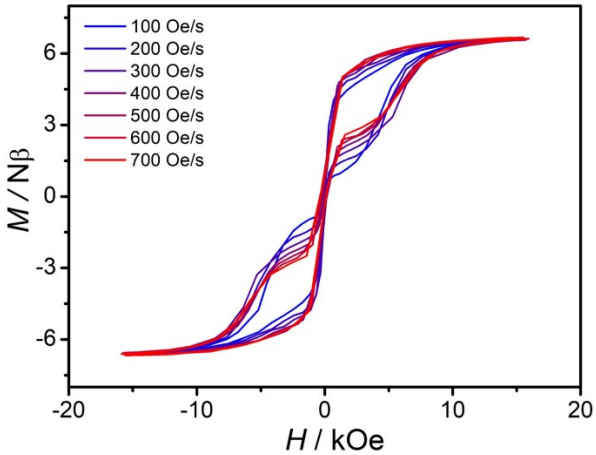

Fig. S19 Magnetic hysteresis loops of **1** at the indicated field sweep rates and at 2 K.

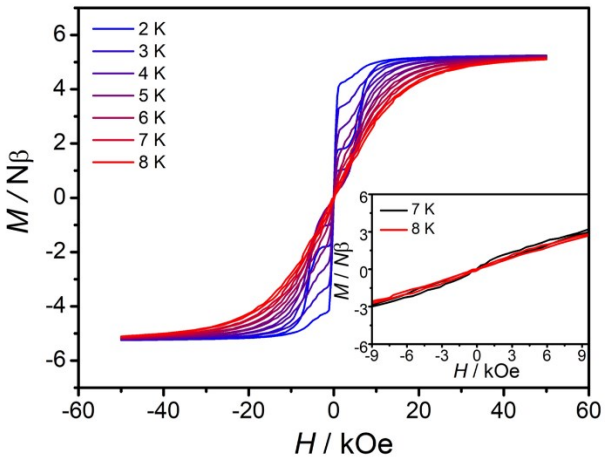

Fig. S20 Magnetic hysteresis loops of **2** at a field sweep rate of 0.02 T Oe s^{-1}.

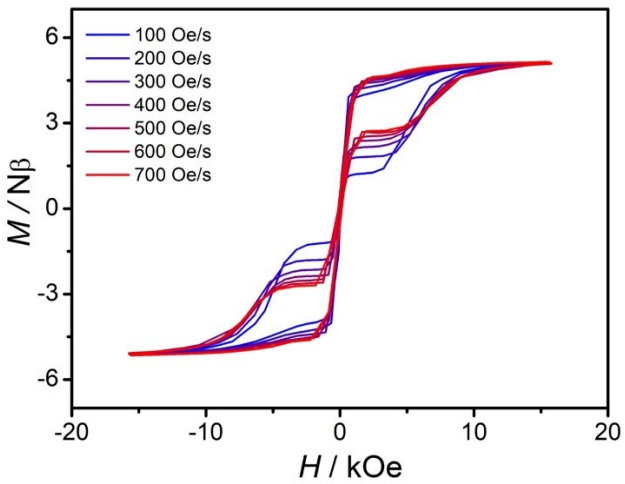

Fig. S21 Magnetic hysteresis loops of **2** at the indicated field sweep rates and at 2 K.

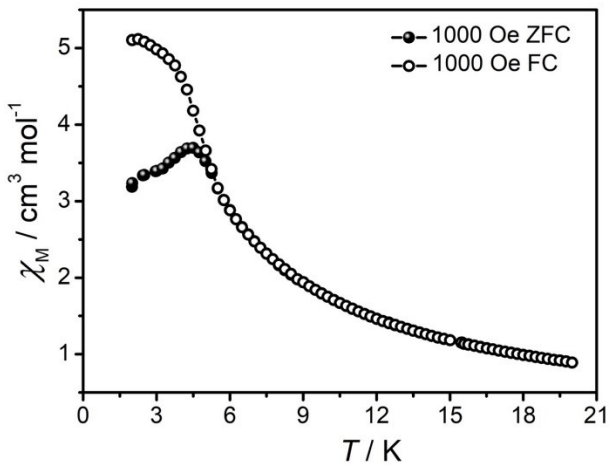

Fig. S22 FC/ZFC magnetizations at 1000 Oe for **1**.

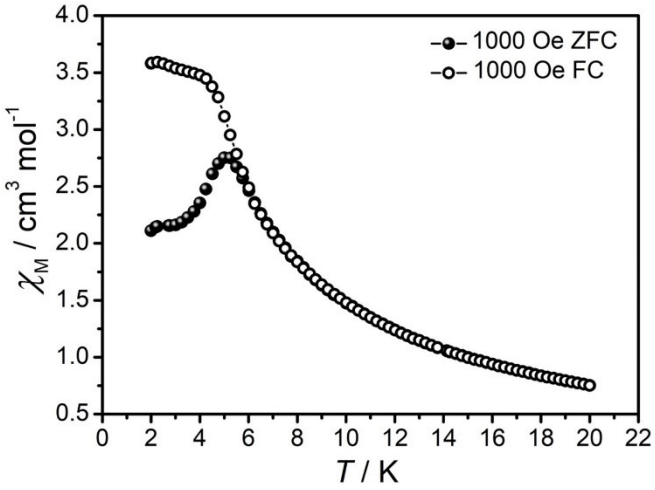

Fig. S23 FC/ZFC magnetizations at 1000 Oe for **2**.

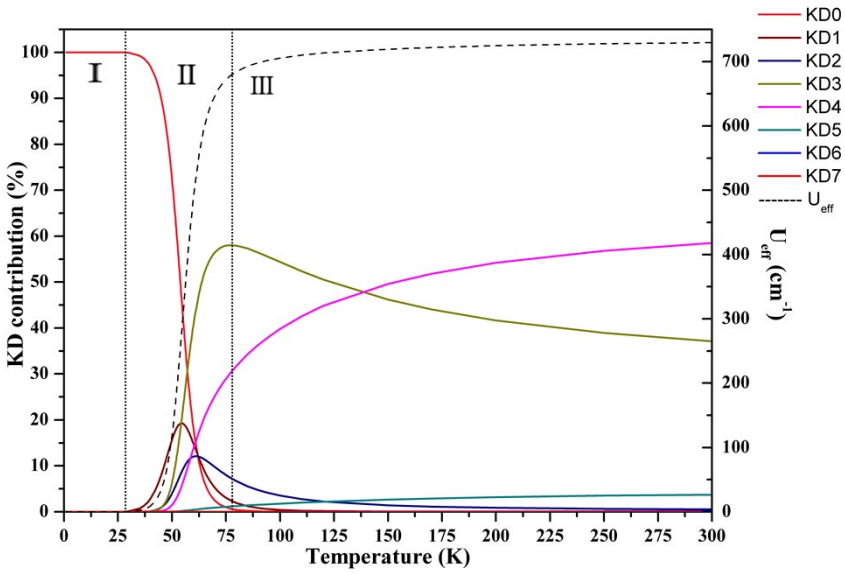

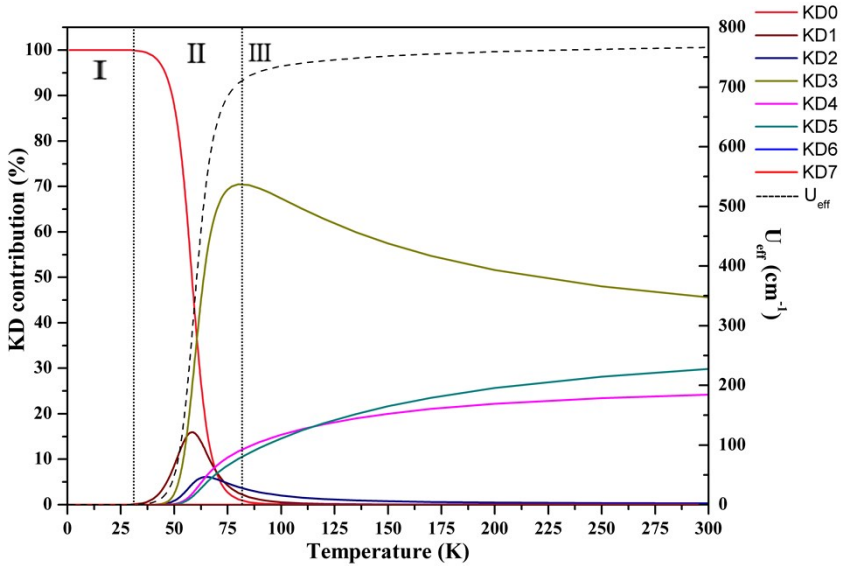

Fig. S24 Predicted effective barrier and relaxation contributions from various KDs of **1** (up) and **2** (down). U_{eff} is represented as a dashed black line, and its value is indicated on the right *y*-axis. The left *y*-axis represents the relative contribution of each KD to relaxation.

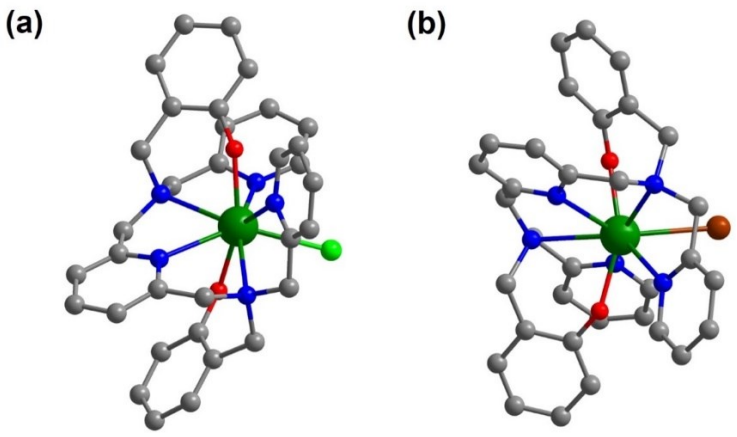

Fig. S25 Calculated complete structures of **1** (a) and **2** (b); Color code: Dy (green), O (red), N (blue), C (grey), Cl (bright green), Br (sorrel). Hydrogen atoms are omitted for clarity.

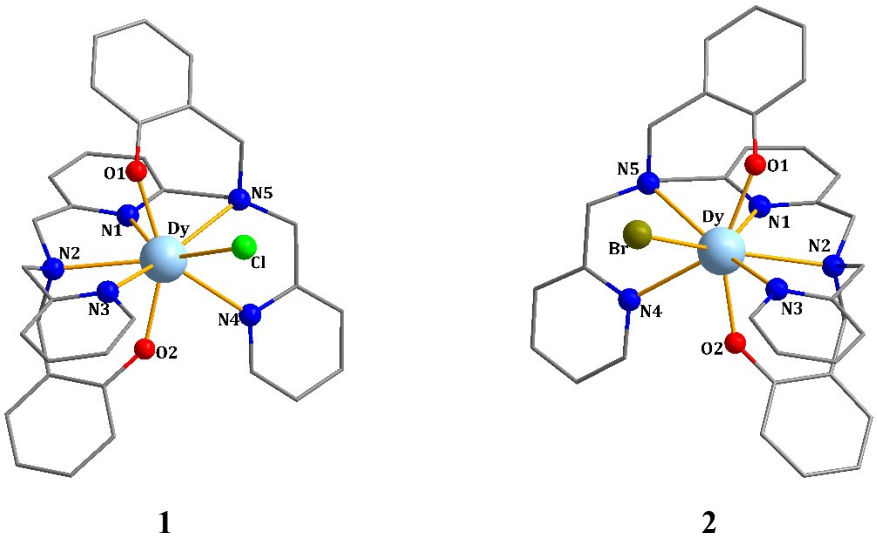

1 **2**

Fig. S26 Labeled molecular structures for **1** and **2**.

S5. Tables

Table S1 Crystal Data and Structure Refinement Details of **1** and **2**.

Compounds	**1**	**2**
Formula	$C_{34}H_{36}ClDyN_5O_3$	$C_{37}H_{39}BrDyN_5O_3$
Formula wt	750.61	844.14
Temperature (K)	293	293
Crystal System	orthorhombic	orthorhombic
Space Group	Pbca	Pbca
a (Å)	14.8133(4)	18.7957(8)
b (Å)	24.4403(7)	14.9643(6)
c (Å)	18.4864(5)	24.8780(13)
α (deg)	90	90
β (deg)	90	90
γ (deg)	90	90
Z	8	8
V (Å^3)	6692.8(3)	6997.3(5)
ρ_{calc} (g/cm^3)	1.490	1.603
μ (mm^{-1})	2.351	3.321
F(000)	3008.0	3368.0
R_{int}	0.0521	0.0879
Goodness-of-fit on F^2	1.041	0.981
R_1,wR_2 (I >2σ(I))[a]	0.0494, 0.1313	0.0532, 0.1185
R_1,wR_2 (all data)[b]	0.0601, 0.1371	0.1047, 0.1399

$${}_{a}R_1 = \sum \left| |F_O| - |F_C| \right| / \sum |F_O|, \quad {}_{b}wR_2 = \left| \sum w\left(|F_O|^2 - |F_c|^2\right) \right| / \sum \left| w(F_o)^2 \right|^{1/2}$$

Table S2 Selected Bond Lengths (Å) and Bond Angles (deg) for **1** and **2**.

1				**2**			
Bond Lengths around Dy1 (Å)				**Bond Lengths around Dy1 (Å)**			
Dy1-O1	2.225(4)	Dy1-N2	2.657(5)	Dy1-O1	2.196(5)	Dy1-N2	2.664(6)
Dy1-O2	2.186(4)	Dy1-N3	2.649(5)	Dy1-O2	2.226(5)	Dy1-N3	2.701(6)
Dy1-Cl1	2.710(2)	Dy1-N4	2.629(5)	Dy1-Br1	2.875(1)	Dy1-N4	2.673(6)
Dy1-N1	2.559(5)	Dy1-N5	2.696(5)	Dy1-N1	2.574(6)	Dy1-N5	2.620(6)
Bond angles around Dy1 (°)				**Bond angles around Dy1 (°)**			
O1-Dy1-O2	150.35(15)			O1-Dy1-O2	150.10(17)		
O1-Dy1-Cl1	88.10(11)			O1-Dy1-Br1	88.07(12)		
O1-Dy1-N1	72.28(15)			O1-Dy1-N1	72.21(19)		
O1-Dy1-N2	79.77(14)			O1-Dy1-N2	78.10(19)		
O1-Dy1-N3	78.42(15)			O1-Dy1-N3	139.66(19)		
O1-Dy1-N4	87.99(16)			O1-Dy1-N4	78.72(18)		
O1-Dy1-N5	140.03(15)			O1-Dy1-N5	87.79(19)		
O2-Dy1-Cl1	107.99(13)			O2-Dy1-Br1	108.56(13)		
O2-Dy1-N1	104.51(16)			O2-Dy1-N1	104.03(19)		
O2-Dy1-N2	72.50(15)			O2-Dy1-N2	128.21(19)		
O2-Dy1-N3	127.98(16)			O2-Dy1-N3	69.42(19)		
O2-Dy1-N4	71.38(16)			O2-Dy1-N4	73.06(18)		
O2-Dy1-N5	68.95(15)			O2-Dy1-N5	71.85(19)		

Symmetry operation codes: [#1] 0.5-X,-Y, 0.5+Z; [#2] -X, 0.5+Y, 0.5-Z; [#3] 0.5+X, 0.5-Y, -Z.

Table S3 Symmetries and Deviated CSM Parameters for **1**.

Label	Shape	Symmetry	Deviated value
OP-8	Octagon	D_{8h}	29.553
HPY-8	Heptagonal pyramid	C_{7v}	20.553
HBPY-8	Hexagonal bipyramid	D_{6h}	14.412
CU-8	Cube	O_h	13.340
SAPR-8	Square antiprism	D_{4d}	6.102
TDD-8	Triangular dodecahedron	D_{2d}	4.086
JGBF-8	Johnson gyrobifastigium J26	D_{2d}	11.391
JETBPY-8	Johnson elongated triangular bipyramid J14	D_{3h}	24.775
JBTPR-8	Biaugmented trigonal prism J50	C_{2v}	3.404
BTPR-8	Biaugmented trigonal prism	C_{2v}	2.997
JSD-8	Snub diphenoid J84	D_{2d}	4.129
TT-8	Triakis tetrahedron	T_d	13.997
ETBPY-8	Elongated trigonal bipyramid	D_{3h}	21.841

Table S4 Symmetries and Deviated CSM Parameters for **2**.

Label	Shape	Symmetry	Deviated value
OP-8	Octagon	D_{8h}	29.853
HPY-8	Heptagonal pyramid	C_{7v}	20.629
HBPY-8	Hexagonal bipyramid	D_{6h}	14.473
CU-8	Cube	O_h	13.206
SAPR-8	Square antiprism	D_{4d}	6.131
TDD-8	Triangular dodecahedron	D_{2d}	4.237
JGBF-8	Johnson gyrobifastigium J26	D_{2d}	11.679
JETBPY-8	Johnson elongated triangular bipyramid J14	D_{3h}	25.267
JBTPR-8	Biaugmented trigonal prism J50	C_{2v}	3.455
BTPR-8	Biaugmented trigonal prism	C_{2v}	2.984
JSD-8	Snub diphenoid J84	D_{2d}	4.500
TT-8	Triakis tetrahedron	T_d	13.671
ETBPY-8	Elongated trigonal bipyramid	D_{3h}	21.867

Table S5 Debye Model Fitting Parameters for **1** at zero dc field.

T / K	χ_S / cm^3 mol^{-1}	χ_T / cm^3 mol^{-1}	τ / s	α
2	3.11E-04	7.24561	0.01180	0.24736
4	3.49E-04	3.95551	0.01463	0.26068
6	0.05016	2.68832	0.01503	0.23939
8	0.04414	2.04733	0.01400	0.22804
10	0.0429	1.64485	0.01217	0.20323
12	0.04173	1.36885	0.00997	0.17306
14	0.0396	1.16961	0.00799	0.14483
16	0.03568	1.02388	0.00643	0.12285
18	0.03018	0.90844	0.00521	0.10729
20	0.02863	0.81652	0.00420	0.09234
22	0.02512	0.74254	0.00337	0.08443
24	0.02979	0.67962	0.00279	0.06895
26	0.02163	0.62729	0.00229	0.0668
28	0.01925	0.58378	0.00193	0.06127
30	0.01768	0.54475	0.00164	0.05314
32	0.01665	0.51072	0.00139	0.04549
34	0.02064	0.48028	0.00120	0.03172
36	6.48E-10	0.45419	9.66236E-4	0.03970
38	8.42E-10	0.43228	8.08729E-4	0.05058
40	1.51E-09	0.40882	6.70358E-4	0.02451
42	1.86E-09	0.39055	5.42352E-4	0.03156
44	2.46E-09	0.37369	4.28914E-4	0.03243
46	1.75E-09	0.35749	3.2887E-4	0.02819
48	1.85E-09	0.34314	2.41303E-4	0.02773
50	2.41E-09	0.33047	1.59601E-4	0.04306
52	3.63E-09	0.31706	1.11793E-4	0.01746
54	5.42E-09	0.30518	7.89742E-5	0.01682

Table S6 Debye Model Fitting Parameters for **2** at zero dc field.

T / K	χ_S / cm^3 mol^{-1}	χ_T / cm^3 mol^{-1}	τ / s	α
2	1.80845E-7	6.58909	0.01384	0.24795
4	2.07528E-7	3.56722	0.01681	0.26060
6	2.55278E-7	2.44071	0.01711	0.26153
8	3.23813E-7	1.86359	0.01616	0.25336
10	2.30531E-7	1.50000	0.01422	0.23511
12	3.87191E-7	1.24472	0.01201	0.21286
14	5.98271E-7	1.06916	0.01008	0.19037
16	1.05093E-6	0.92543	0.00826	0.16386
18	1.85118E-6	0.83394	0.00703	0.15382
20	3.23353E-6	0.74514	0.00584	0.13431
22	5.83673E-6	0.66938	0.00481	0.11415
24	1.06213E-5	0.61713	0.00406	0.10699
26	0.01727	0.56578	0.00353	0.06873
28	0.01548	0.52467	0.00295	0.05887
30	0.01383	0.49087	0.00248	0.05581
32	0.01114	0.46243	0.00208	0.05658
34	0.01203	0.43005	0.00172	0.03893
36	0.00999	0.40736	0.00143	0.03876
38	0.00808	0.38812	0.00118	0.04175
40	0.00722	0.37000	9.62256E-4	0.03953
42	0.01932	0.34680	7.92967E-4	0.00280
44	0.00907	0.33231	6.01415E-4	0.01808
46	0.01013	0.31971	4.63649E-4	0.01808
48	0.00566	0.30613	3.32397E-4	0.01731
50	0.01531	0.29536	2.4753E-4	0.00732
52	0.0238	0.28441	1.71024E-4	0.00631

Table S7 Calculated energy levels (cm^{-1}), ***g*** (g_x, g_y, g_z) tensors and predominant m_J values of the lowest eight KDs of **1** and **2** using CASSCF/RASSI-SO[3] with MOLCAS 8.4[2].

KDs	**1**			**2**		
	E/cm^{-1}	***g***	m_J	E/cm^{-1}	***g***	m_J
1	0.0	0.001 0.001 19.869	±15/2	0.0	0.001 0.001 19.866	±15/2
2	278.3	0.028 0.035 17.081	±13/2	287.5	0.016 0.020 17.091	±13/2
3	521.6	0.405 0.542 14.001	±11/2	539.7	0.185 0.214 14.133	±11/2
4	678.9	4.008 6.218 8.638	±9/2	710.6	3.036 3.958 10.112	±9/2
5	758.9	9.150 6.450 1.146	±5/2	798.7	0.887 3.929 8.138	±5/2
6	795.8	1.342 3.239 14.026	±1/2	826.2	1.560 5.694 12.521	±1/2
7	854.1	0.340 0.650 17.711	±3/2	883.1	0.161 0.403 17.749	±3/2
8	970.2	0.046 0.099 19.439	±7/2	987.4	0.084 0.188 19.371	±7/2

Table S8 Wave functions with definite projection of the total moment | m_J > for the lowest eight KDs for **1** and **2** and the included θ angles of magnetic axes between the excited KD and the ground KD.

	E/cm^{-1}	wave functions	θ/degree
1	0.0	99.7%|±15/2>	0.0
	278.3	97.2%|±13/2>	6.3
	521.6	87.1%|±11/2>+5.3%|±9/2>	8.5
	678.9	55.9%|±9/2>+14.5%|±5/2>+12.0%|±7/2>+8.7%|±3/2>	19.6
	758.9	28.6%|±1/2>+22.2%|±7/2>+17.4%|±3/2>+16.9%|±5/2> +10.5%|±9/2>	20.7
	795.8	28.8%|±3/2>+27.8%|±1/2>+17.6%|±7/2>+12.6%|±5/2> +12.2%|±9/2>	91.4
	854.1	25.8%|±1/2>+25.6%|±5/2>+24.8%|±3/2>+17.7%|±7/2>	97.5
	970.2	30.0%|±5/2>+26.2%|±7/2>+19.9%|±3/2>+12.0%|±1/2> +10.1%|±9/2>	70.5
2	0.0	99.7%|±15/2>	0.0
	287.5	97.6%|±13/2>	5.9
	539.7	89.1%|±11/2>+4.9%|±9/2>	8.5
	710.6	65.0%|±9/2>+13.1%|±7/2>+11.0%|±5/2>+6.4%|±3/2>	17.0
	798.7	28.6%|±7/2>+27.6%|±5/2>+24.4%|±1/2>+9.5%|±3/2>	56.5
	826.2	39.0%|±3/2>+35.7%|±1/2>+12.5%|±7/2>+7.4%|±9/2>	94.2
	883.1	28.1%|±1/2>+25.2%|±3/2>+25.0%|±5/2>+15.5%|±7/2>	82.6
	987.4	31.6%|±5/2>+26.7%|±7/2>+19.7%|±3/2>+10.5%|±1/2> +9.7%|±9/2>	70.2

Table S9 Calculated crystal-field parameters *B(k,q)* for **1** and **2**.

k	*q*	**1**	**2**
2	−2	0.1147×10^{1}	−0.9657
	−1	0.1706×10^{1}	0.1709×10^{1}
	0	-0.4951×10^{1}	-0.5168×10^{1}
	1	0.1862×10^{1}	-0.1804×10^{1}
	2	0.1526×10^{1}	0.1416×10^{1}
4	−4	0.3642×10^{-2}	-0.5161×10^{-2}
	−3	0.2070×10^{-1}	0.2054×10^{-2}
	−2	-0.4883×10^{-2}	0.9662×10^{-1}
	−1	-0.7287×10^{-2}	-0.7316×10^{-3}
	0	-0.6758×10^{-2}	-0.6685×10^{-2}
	1	-0.9325×10^{-2}	0.9809×10^{-2}
	2	0.8572×10^{-2}	0.8713×10^{-2}
	3	0.1135×10^{-1}	0.1205×10^{-2}
	4	0.6426×10^{-2}	0.1595×10^{-2}
6	−6	-0.2118×10^{-3}	0.1420×10^{-3}
	−5	0.6296×10^{-3}	0.5891×10^{-3}
	−4	-0.1012×10^{-3}	0.8821×10^{-4}
	−3	-0.6822×10^{-4}	0.5878×10^{-5}
	−2	-0.9579×10^{-4}	0.1220×10^{-3}
	−1	-0.8116×10^{-4}	-0.8224×10^{-4}
	0	0.2856×10^{-4}	0.2829×10^{-4}
	1	-0.4661×10^{-4}	0.3775×10^{-4}
	2	-0.8074×10^{-4}	-0.5138×10^{-4}
	3	0.1360×10^{-3}	-0.1344×10^{-3}
	4	-0.6935×10^{-5}	0.6124×10^{-4}
	5	0.3077×10^{-3}	0.2704×10^{-3}
	6	-0.4796×10^{-4}	0.1537×10^{-3}

Table S10 Calculated LoProp charges per atoms in the ground state of **1** and **2** using CASSCF/RASSI with MOLCAS 8.4.

		1		**2**
Easy axis	Dy	2.440	Dy	2.426
	O1	–0.911	O1	–0.919
	O2	–0.933	O2	–0.935
	Average	–0.922	Average	–0.927
Hard plane	N1	–0.386	N1	–0.382
	N2	–0.308	N2	–0.310
	N3	–0.352	N3	–0.353
	N4	–0.350	N4	–0.355
	N5	–0.316	N5	–0.315
	Cl	–0.196	Br	–0.865
	Average	–0.318	Average	–0.430

S6. References

1 (a) G. M. Sheldrick, *SHELXL-97, Program for Refinement of Crystal Structures*, University of Göttingen: Göttingen, Germany, 1997; (b) Sheldrick, G. M, *SHELXS-97, Program for Solution of Crystal Structures*, University of Göttingen: Göttingen, Germany, 1997; (c) G. M. Sheldrick, A short history of *SHELX*, *Acta Crystallogr., Sect. A: Found. Crystallogr.*, 2008, **64**, 112–; (b) O. V. Dolomanov, L. J. Bourhis, R. J. Gildea, J. A. K. Howard and H. Puschmann, OLEX2: a complete structure solution, refinement and analysis program, *J. Appl. Cryst.*, 2009, **42**, 339–341; (c) G. M. Sheldrick, High-pressure synchrotron radiation crystallography, from organic conductors to chemistry in the lower mantle, *Acta Crystallogr., Sect. C: Struct. Chem.*, 2015, **71**, 3.

2 F. Aquilante, J. Autschbach, R. K. Carlson, L. F. Chibotaru, M. G. Delcey, L. De Vico, I. Fdez. Galván, N. Ferré, L. M. Frutos, L. Gagliardi, M. Garavelli, A. Giussani, C. E. Hoyer, G. Li Manni, H. Lischka, D. Ma, P. Å. Malmqvist, T. Müller, A. Nenov, M. Olivucci, T. B. Pedersen, D. Peng, F. Plasser, B. Pritchard, M. Reiher, I. Rivalta, I. Schapiro, J. Segarra-Martí, M. Stenrup, D. G. Truhlar,

L. Ungur, A. Valentini, S. Vancoillie, V. Veryazov, V. P. Vysotskiy, O. Weingart, F. Zapata and R. Lindh, MOLCAS 8: New Capabilities for Multiconfigurational Quantum Chemical Calculations across the Periodic Table, *J. Comput. Chem.*, 2016, **37**, 506–541.

3 (a) L. F. Chibotaru, L. Ungur and A. Soncini, The Origin of Nonmagnetic Kramers Doublets in the Ground State of Dysprosium Triangles: Evidence for a Toroidal Magnetic Moment, *Angew. Chem. Int. Ed.*, 2008, **47**, 4126–4129; (b) L. Ungur, W. Van den Heuvel and L. F. Chibotaru, Ab initio investigation of the non-collinear magnetic structure and the lowest magnetic excitations in dysprosium triangles, *New J. Chem.*, 2009, **33**, 1224–1230; (c) L. F. Chibotaru, L. Ungur, C. Aronica, H. Elmoll, G. Pilet and D. Luneau, Structure, Magnetism, and Theoretical Study of a Mixed-Valence $Co^{II}_3Co^{III}_4$ Heptanuclear Wheel: Lack of SMM Behavior despite Negative Magnetic Anisotropy, *J. Am. Chem. Soc.*, 2008, **130**, 12445–12455.

4 (a) X. L. Liu, Z. H. Wei, B. B. Xu and X. M. Liu, A heptadentate ligand possessing two phenol groups: Its diverse coordination chemistry and the catalytic behaviours of its transition complexes towards benzene oxidation, *Polyhedron*, 2014, **81**, 743–748; (b) X. L. You, Z. H. Wei, H. L. Wang, D. P. Li, J. Liu, B. B. Xu and X. M. Liu, Synthesis of two copper clusters and their catalysis towards the oxidation of benzene into phenol, *RSC Adv.*, 2014, **4**, 61790–61798.